Final Technical Report

Quantifying the effect of ductile and brittle material properties on southern California crustal deformation: PyLith finite-element models

USGS Award Number: G20AP00013

PI: Elizabeth Hearn,
Consulting Geophysicist, dba HEARN, ELIZABETH
21 Valley Oak Street, Portola Valley CA 94028
(408) 334-8075
hearn.liz@gmail.com

Term covered by the award: Jan 1 - Dec 31, 2020

Acknowledgement of Support and Disclaimer: This material is based upon work supported by the U.S. Geological Survey under Grant No. G20AP00013. The views and conclusions contained in this document are those of the author and should not be interpreted as representing the opinions or policies of the U.S. Geological Survey. Mention of trade names or commercial products does not constitute their endorsement by the U.S. Geological Survey.

Abstract

I have developed static deformation models of the southern California lithosphere using the Computational Infrastructure for Geodynamics (CIG) finite-element code PyLith (Aaagaard et al., 2017). These models incorporate a range of ductile material distributions for the lower crust and upper mantle, including layers, layers plus a vertical SAF shear zone, and 3D viscosity from the Southern California Earthquake Center (SCEC) community rheology model (CRM). Ductile materials are represented with Maxwell and/or Burgers viscoelastic rheologies. Model meshes representing the San Andreas fault (SAF) in northern and southern California are used to calculate postseismic and seismic-cycle deformation associated with large SAF earthquakes. As expected, models incorporating Burgers viscoelasticity in the lower crust and upper mantle give larger postseismic velocities than equivalent models incorporating Maxwell viscoelasticity. Seismic-cycle models incorporating Burgers rheology yield larger perturbations or "ghost transients" contributing to present-day surface velocities around the SAF, which bias geodetic estimates of SAF slip rates to lower values. Viscosity heterogeneities are influential insofar as they affect viscosities close to the ruptures: postseismic and seismic-cycle velocities appear to be insensitive to viscosity variations in the far field. My 2020 work provides a foundation for ongoing explorations of seismic-cycle and long-term deformation associated with the San Andreas and other western U.S. faults.

Report

For 2020, I described four operational tasks and two scientific questions to address once the tasks were complete. The tasks were:

> (T1) Develop a reference model of the southern California lithosphere incorporating an elastic upper crust over uniform lower crust and upper mantle layers, and faults;
> (T2) Populate a copy of the reference model with CRM ductile properties, incorporating temperatures from the CTM;
> (T3) Populate a copy of the reference model *and* the model from (2) with three-dimensionally varying elastic properties and density based on an old version of the SCEC community velocity model (CVM-H 5.3); and
> (T4) Generate gravitational pre-stresses from the density distribution in (3).

After completing these tasks, I proposed to:

> (S1) Assess sensitivity of modeled deformation to rheological parameters by comparing modeled coseismic and postseismic deformation resulting from hypothetical shear dislocations;
> and
> (S2) Compare GPS postseismic velocity data from the 1999 Hector Mine earthquake with velocities from models incorporating SCEC CTM temperatures and CRM rheologies.

I completed T1 and T2 for the southern California model, with the implementation of the CRM into the southern California model absorbing significant time. (Note that this is distinct from my SCEC-funded research, leading the development of the CRM). Instead of proceeding with T3 and T4, I developed a model of the northern San Andreas Fault. This was done to calculate a GPS velocity field correction prior to geodetic slip rate inversion modeling for the 2023 USGS NSHMP, which was scheduled to begin in January 2021. I began work on assessing model sensitivity to viscous material parameters, with an emphasis on heterogeneity and Burgers material properties, some preliminary results are described here. The Hector Mine earthquake postseismic modeling was paused after I determined that GPS data could provide just a rough check on CRM rheologies. Given uncertainties in Burgers viscoelastic model parameters, and even uncertainties about whether two relaxation times are sufficient to describe postseismic deformation over decadal timescales (e.g. Ivins et al., 2020), any comparisons with CRM viscosities would be qualitative.

Meshes and fault parameters

Southern California mesh. At the beginning of 2020, a preliminary PyLith model mesh of southern California had been generated from the GAEA finite-element model mesh from Hearn (2019). This mesh was unstructured, comprised of quadrilateral elements, and 1200 by 1600 km by 70 km (six layers) in dimension. Elements along major faults at the center of the model were about 2-5 km in dimension, increasing in size with distance from the central part of the model. Nodes falling along major faults were not yet activated at the start of the grant period. During 2020, I extended this mesh to a depth of 600 km (22 model layers), activated fault nodes representing the San Andreas Fault, and populated elements with elastic and viscous parameters. The mesh was also modified to include a viscous shear zone 5-10 km (4 elements) wide, extending the SAF downward to the mantle asthenosphere. The current mesh comprises 428,384 elements.

The SAF as represented in this model consists of the Big Bend, Mojave and San Bernardino segments, which ruptured in 1857 and 1812 (Scharer and Streig, 2019, Figure 2). It is 300 km long and extends from lat 34.04 to lat 35.33. For the seismic cycle modeling, I assign 4.4 m slip per event, tapering to 2 m at the south end of the San Bernardino segment, per Scharer and Yule, 2020 (ellipses on their Figure 3). This slip is consistent with a 130-year recurrence interval (inferred from Scharer and Yule, 2020, Figure 3) and a slip rate of 34 mm/yr, tapered to 15 mm/yr along the San Bernardino Fault (consistent with UCERF3 slip rates; Field et al., 2013). Modeled slip is uniform from 0 to 14 km, linearly tapering to 0 at 24 km depth. The same slip distribution is used for postseismic deformation models shown on Figure 2.

Timing of modeled earthquakes since 980 AD is loosely based on the Scharer and Yule (2020) maximum rupture model. Ruptures that were spaced closely in time, and which together ruptured most of the 1857 + 1812 rupture area, are lumped together in the calculation, resulting in eight modeled events: 1857 (and 1812), 1720, 1550, 1470, 1350, 1200, 1100 and 980 AD. To address model sensitivity to timing uncertainties and to my somewhat ad-hoc lumping of events, I also ran models with regular 130-year recurrence intervals, ending with the 1857 earthquake.

Northern California mesh. Near the end of the grant period, I developed a PyLith model mesh representing the San Andreas fault in northern California. This model is 1600 by 2000 km and 750 km (34 model layers) deep. Like the southern CA mesh it is unstructured, with element dimensions of 2-3 km along the San Andreas fault. The mesh is designed with upper crust and lower crust/mantle domains, and a viscous shear zone domain 5-10 km (4 elements) wide extends the SAF downward to the mantle asthenosphere. The current mesh comprises 229,840 elements.

The mesh is currently set up to model seismic cycles or postseismic deformation. The 1906 SAF rupture segment represented is 470 km long, extending from 36.51 to 40.72 latitude (e.g., Song et al., 2008). Uniform slip is modeled from surface to 15 km depth, linearly tapering to 0 at 20 km. Coseismic slip is 4.8 m on all but Santa Cruz Mts section where slip tapers to 3.2 m. The interseismic interval is assumed to be 200 yr (within the range of 200-250 yr from Scharer and Streig, 2019). This gives a slip rate of 24 mm/yr (e.g., Field et al., 2013), except for the Santa Cruz Mountain segment (16 mm/yr). This segment has smaller events between the 1906-like earthquakes (e.g. events in 1838 and 1890; Streig et al., 2020). These will be added to the model in 2021, increasing the slip rate of this segment.

Timing of earthquakes since 800 AD was loosely based on the chronology of Scharer and Streig (2019). Ruptures that were spaced closely in time, and which together ruptured most of the 1906 rupture area, were lumped into single modeled events (in 1906, 1750, 1400, 1100, 1000, and 800 AD). A recurrence interval of 200 years was assumed prior to 800 AD. To address model sensitivity to timing uncertainties and to my choices in lumping of events, I also ran models with regular 200-year recurrence intervals, ending with the 1906 earthquake. Other variations in earthquake timing and slip distribution are being explored.

Populating Meshes with Material Properties

Elastic parameters. Both the northern and southern CA meshes currently incorporate 1D elastic structure. The elastic moduli are computed from Vp, Vs, and density from the Hadley-Kanamori 1D model, which is the background model for SCEC CVM-H (https://strike.scec.org/scecpedia/CVM-H_User_Guide). 3D elastic properties from the SCEC CVM will be incorporated into the southern California mesh in 2021.

Viscous parameters. Several suites of viscoelastic models have been developed, incorporating reasonable rheologies based on various published studies (e.g. Pollitz, 2019). Geometrically, these can be categorized as layered models, layered models with a ductile shear zone extending the SAF downward to the mantle asthenosphere, and for southern California, a fully 3D viscoelastic model based on the SCEC CRM.

Within each category, Maxwell or Burgers rheologies are modeled. The Maxwell viscoelastic rheology is described with two parameters: viscosity η and shear modulus μ. The Burgers

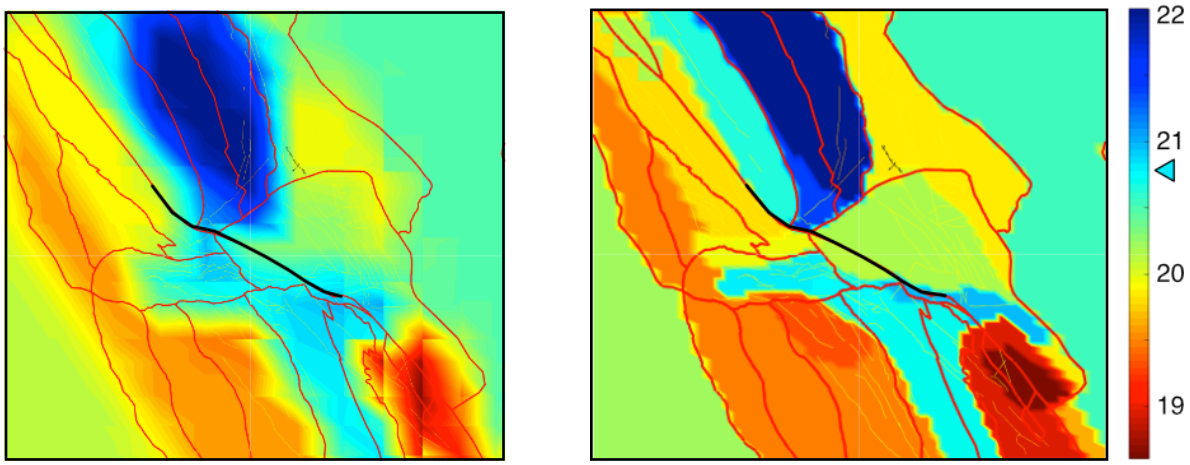

Figure 1. Effective viscosities at a depth of 42 km from the SCEC Community rheology model. Colors show log of effective viscosity, red lines are CRM province boundaries, and black line is the modeled southern SAF rupture. (left) coarse resolution version used in the PyLith models, (right) finer resolution version to be used in future models. The cyan pointer on the colorbar shows the CRM-wide average viscosity at 42 km depth.

rheology requires two additional parameters: the ratio of transient (Kelvin element) viscosity to steady-state (Maxwell) viscosity (R_B); and the ratio of μ to the shear modulus for the Kelvin element (Δ_{bar}). These parameters govern the magnitude and duration of transient viscosity evolution toward the higher Maxwell value, but they are poorly constrained. Ivins et al. (2020) summarizes Burgers material parameters used in (or inferred from) several modeling studies. Many of these studies assume that Δ_{bar} is 1 and R_B is 0.1, though laboratory experiments suggest ranges of 0.05 to 0.36, and 0.17 to 0.67, respectively (Chopra, 1997). For all models, I assume as a default that Δ_{bar} is 0.2 and R_B is 0.2, though other values are explored to assess sensitivity. PyLith does not represent Burgers materials directly. I used equations from Müller (1986) to set PyLith generalized Maxwell material parameters to values that represent the desired Burgers materials.

Northern California Model. For Maxwell viscoelastic models, lower crust and mantle Maxwell viscosities are depth-dependent and based on Pollitz (2019) assuming strain rate = 10^{-14}/s. The minimum Maxwell viscosity for the mantle is set to 5 x 10^{18} Pa s from 80 km to the bottom of the model. Upper crust Maxwell viscosity is 10^{24} Pa s to make it essentially elastic. The lower crust mean viscosity is about 1 - 3 x 10^{20} Pa s. Shear zone effective viscosity at most depths is 2 x 10^{18} Pa s, rapidly transitioning to the upper crustal value of 10^{24} Pa s at 13-17 km depth. SAF shear zone viscosity per unit width (~10^{14} - 10^{15} Pa s /m) is consistent with Kenner and Segall (2003) and Vaghri (2011) but lower than Johnson and Segall (2004). Burgers material properties include the Maxwell viscosity and the shear modulus; additional parameters R_B and Δ_{bar} are assigned as described in the previous section.

Southern California Model. Two sets of models with layered viscosity structures were developed: one with the same values used for the northern SAF model, and another set with mean viscosity values at each depth computed from the SCEC CRM. The viscous shear zone Maxwell viscosities are the same as for the southern CA SAF shear zone.

A third model suite incorporates both 3D viscoelastic structure and a viscous shear zone. To generate effective viscosities from the SCEC CRM, I sampled CTM temperature and CRM geologic framework lithology at points on a 3D grid, then used these together with CRM aggregate rock flow laws and assumed strain rates to calculate effective viscosities. Fine and coarse regular grids with effective viscosities were converted into PyLith spatial database files. For the models presented here, I assumed a strain rate of 5×10^{-15} /s, except in the Great Basin, Pacific Ocean, and Sierra Nevada regions where I assumed a lower strain rate (10^{-15} /s). The CRM and CTM are not defined for depths exceeding 100 km, so viscosity values at 100 km were extruded downward to the bottom model boundary. Burgers material properties for the lower crust, mantle, and ductile shear zone are assigned using the Maxwell viscosity, shear modulus, and parameters R_B and Δ_{bar} as described in the previous section.

Postseismic and seismic cycle model results

Several suites of postseismic and seismic cycle models for large earthquakes on the northern and southern SAF have been run, exploring Maxwell and Burgers rheologies, and layered vs. heterogeneous properties. Two examples are given here.

The first example (**Figure 2**) shows postseismic deformation five years after a modeled M 7.8 southern SAF earthquake, assuming slip as described in the "Meshes and fault parameters" section. A model with mean CRM effective viscosities at each depth is compared with another in which 3D CRM effective viscosities are assumed. Shear zone material properties are the same in both instances, and the shear zone is modeled as a Burgers material. In these calculations the lower crust and mantle outside the shear zone are Maxwell materials. **Figure 2** shows larger postseismic velocities for the 3D viscosity case, likely because viscosity values near the rupture are below the CRM-wide average values. Other calculations (not shown here) show the effect of the Burgers rheology: more rapid postseismic deformation, especially for larger values of (R_B Δ_{bar}). This is consistent with a slower evolution from the low (Kelvin) viscosity to the higher Maxwell viscosity (e.g. summary in Ivins et al., 2020).

GPS velocity field corrections for viscoelastic seismic cycle-related velocity perturbations (or "ghost transients") associated with northern SAF seismic cycles have been calculated (**Figure 3**) and provided to the USGS as part of the NSHMP project. They are obtained from models in which I simulate 10,000 years of seismic cycles, then compute cycle-average and present-day velocities, and their difference (the "ghost transient"). The cycle-average velocities, which are identical to those for an elastic dislocation creeping at a constant rate below the locked fault, are model-insensitive. The ghost transients reflect how much the velocity field changes between

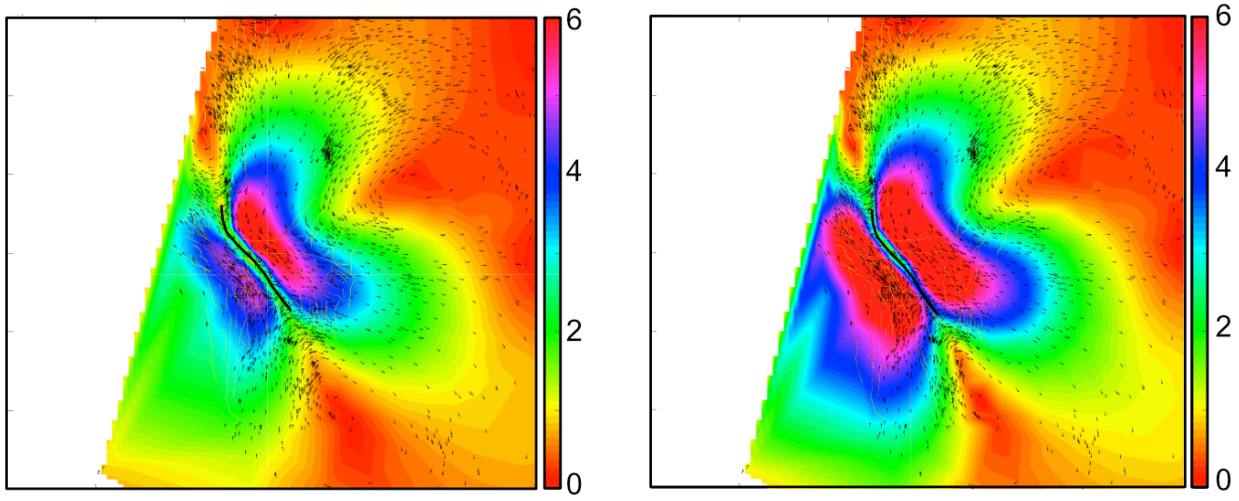

Figure 2. Postseismic velocities five years after a M 7.8 southern SAF earthquake (see text for details). (left) Model with 1D viscous structure representing mean of CRM viscosities at each depth. (right) Model with fully 3D CRM viscosities (see Figure 1 and text for details). Colors indicate velocity magnitudes in mm/yr, arrows show velocity orientations. The 3D model produces larger postseismic velocities because effective viscosities in the neighborhood of the SAF are lower than mean values for the CRM at most depths. These plots are in model coordinates; the y axis (apparent north) is oriented parallel to the Pacific-North America plate boundary (N35W).

large earthquakes, and tend to be larger for short Maxwell relaxation times and long interseismic intervals (e.g. Savage and Prescott, 1978). In both models contributing to **Figure 3**, the lower crust, mantle, and ductile shear zone are treated as Burgers viscoelastic materials, with parameters given in the previous section. For the southern California model, the Maxwell viscosities are from the coarse version of the 3D CRM (**Figure 1**), and the transient viscosities are 1/5 of the Maxwell viscosities (per discussion in the previous section).

Note the left-lateral sense of motion across the SAF in **Figure 3.** When this perturbation is subtracted from the present-day GPS velocity field, larger strain rates around the SAF and higher inferred slip rates will result. This will bring the geodetic rates closer to geological estimates (consistent with, for example, Johnson et al., 2007 and Hearn et al., 2013). The northern SAF has a smaller ghost transient because it is only about 60% of the way through an average seismic cycle (200 years). In contrast, the southern SAF last ruptured in 1857, and the elapsed time since that event exceeds the average recurrence interval.

For both the northern and southern SAF models, representing the irregular timing of earthquakes during the past ~1000 years (rather than assuming a uniform recurrence interval before the most recent earthquake) made little difference to modeled ghost transient amplitudes or orientations. I am continuing to test the robustness of this finding.

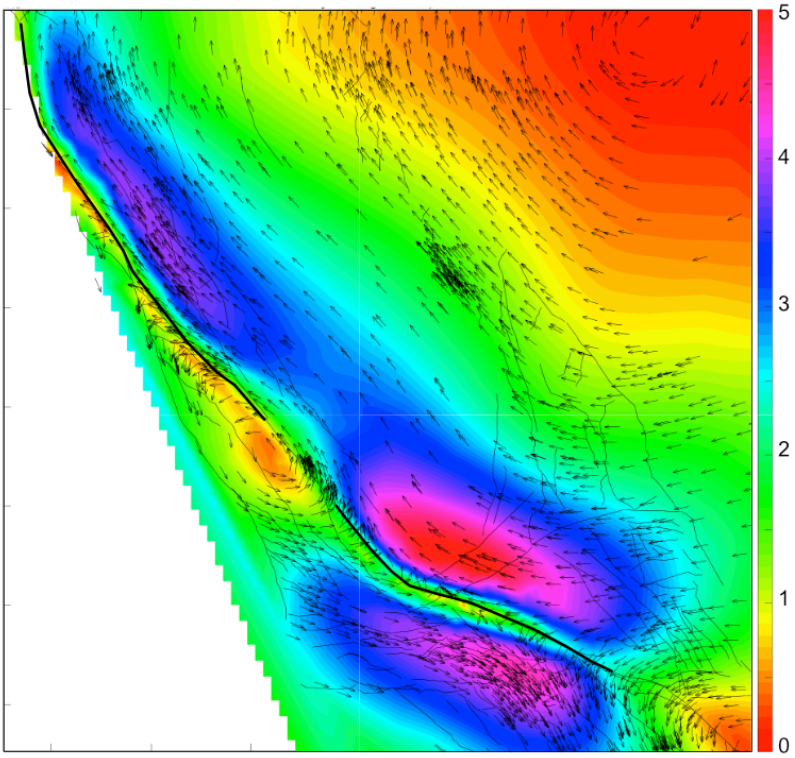

Figure 3. Present-day perturbation to the GPS velocity field in California, due to large earthquakes on the northern and southern San Andreas Fault. Colors and arrows show velocity perturbation magnitudes and orientations, respectively. Thick black lines show modeled northern and southern SAF ruptures. Since both faults are toward the end of (or beyond) their average recurrence intervals, strain rates around them are lower than the long-term average, and the perturbation shows apparent left-lateral motion. When subtracted from the GPS velocity field, this will result in higher apparent strain rates around the faults, and higher slip rates from elastic slip inversions (e.g. Johnson, 2013 and Hearn et al., 2013).

The SAF seismic cycle models were run assuming
Maxwell viscoelasticity, for comparison with the models shown on **Figure 3**. The ghost transient velocities were about 25% smaller, which is expected given less variation in strain rates throughout the seismic cycle. Other calculations suggest that SAF ghost transient magnitudes are more sensitive to variations in lower crust and upper mantle viscosities than to changes in shear zone viscosities. I am still investigating the effect of varying Burgers model parameters Δ_{bar} and R_B on modeled seismic cycle deformation.

References

Aagaard, B., M. Knepley, C. Williams (2017a), PyLith v2.2.1, Computational Infrastructure of Geodynamics, Davis, CA, DOI: 10.5281/zenodo.886600.

Chopra, P. N. (1997), High-temperature transient creep in olivine rocks, Tectonophysics, 279, 93–111, doi:10.1016/S0040-1951(97)00134-0.

Field, E. H. et al. (2013), Uniform California earthquake rupture forecast, version 3 (UCERF3) — The time-independent model: *U.S. Geological Survey Open-File Report 2013–1165*, 97 p., California Geological Survey Special Report 228, http://pubs.usgs.gov/of/ 2013/1165/.

Hearn, E. H., F. F. Pollitz, W. R. Thatcher and C. T. Onishi (2013), How do "ghost transients" from past earthquakes affect GPS slip rate estimates on southern California faults?, Geophys., Geochem., Geosyst., 14, 828–838, doi:10.1002/ ggge.20080.

Hearn, E. and W. Thatcher (2015), Reconciling viscoelastic models of postseismic and interseismic deformation: Effects of viscous shear zones and finite-length ruptures, J. Geophys. Res., *120*(4), 2794-2819.

Hearn, E. H. (2019), Kinematics of southern California crustal deformation: Insights from finite-element models, Tectonophysics, 758, 12-28.

Ivins, E., L. Caron, S. Adhikari, E. Larour and M. Scheinert (2020), A linear viscoelasticity for decadal to centennial time scale mantle deformation, Rep. Prog. Phys., 83, 106801.

Johnson, K. M., and P. Segall (2004), Viscoelastic earthquake cycle models with deep stress−driven creep along the San Andreas fault system, J. Geophys. Res., 109, doi: 10.1029/2004JB003096.

Johnson, K. M., G. E. Hilley, and R. Bürgmann (2007), Influence of lithosphere viscosity structure on estimates of fault slip rate in the Mojave region of the San Andreas fault system, J. Geophys. Res., 112, B07408, doi:10.1029/2006JB004842.

Johnson, K.M. (2013), Slip rates and off-fault deformation in Southern California inferred from GPS data and models. J. Geophys. Res. 118. https://doi.org/10.1002/jgrb. 50365.

Kenner, Shelley J., and Paul Segall (2003), Lower crustal structure in northern California: Implications from strain rate variations following the 1906 San Francisco earthquake, *J. Geophys. Res.,* 108, doi:10.1029/2001JB000189.

Müller, G. (1986), Generalized Maxwell bodies and estimates of mantle viscosity, Geophys. J. Int., 87, 1113–41.

Savage, J. C. and W. H. Prescott (1978), Asthenosphere readjustment and the earthquake cycle, J. Geophys. Res., *83*, 3369-3376.

Scharer, K. and A. Streig (2019), The San Andreas Fault System: Complexities along a Major Transform Fault System and Relation to Earthquake Hazards, Chapter 10 of Transform Plate Boundaries and Fracture Zones, https://doi.org/10.1016/B978-0-12-812064-4.00010-4, Elsevier.

Scharer, K. M. and D. Yule (2020), A maximum rupture model for the southern San Andreas and San Jacinto faults, California, derived from paleoseismic earthquake ages: Observations and limitations, Geophys. Res. Lett., 47, e2020GL088532.

Song, S. G., G. C. Beroza and P. Segall (2008), A Unified Source Model for the 1906 San Francisco Earthquake, Bull. Seis. Soc. Am., 98, 823-831.

Streig, Ashley R., Ray J. Weldon, Glenn Biasi, Timothy E. Dawson, Daniel G. Gavin, and Tom P. Guilderson. "New insights into paleoseismic age models on the northern San Andreas Fault: Charcoal inbuilt ages and updated earthquake correlations." *Bulletin of the Seismological Society of America* 110, no. 3 (2020): 1077-1089.

Thatcher, W. and F. Pollitz (2008), Temporal evolution of continental lithospheric strength in actively deforming regions, *GSA Today,* 18, 4-11, doi: 10.1130/GSAT01804-5A.1.

Vaghri, A. (2011), Viscoelastic finite-element models of the earthquake cycle along plate-boundary faults, UBC PhD Dissertation, https://open.library.ubc.ca/cIRcle/collections/ubctheses/24/items/1.0053367.

Project data

As noted in the report, I populated regular grids with effective viscosity values based on the SCEC CRM and CTM. These grids were converted into PyLith spatial database files and used in my southern California simulations. PyLith spatial database files are *not* model mesh dependent:

they may be used by *anyone* using PyLith to model southern California deformation. I will publish instances of southern California 3D rheology spatial database files on Xenodo and will advertise these products on the CIG PyLith wiki, the SCEC CRM website, and in presentations at CIG, SCEC, and other meetings or workshops. Coarse and fine versions, with Maxwell and Burgers rheology (as represented by PyLith's generalized Maxwell model, per Muller, 1986) will be made available.

Bibliography

Pollitz, F.F. et al. (2021), Fault Slip Rates Contributed by Crustal Deformation Models to the 2023 Update to the National Seismic Hazard Model, Seis. Res. Lett., p. 1451.